ELSEVIER

Journal of Alloys and Compounds 434–435 (2007) 28–31

Journal of ALLOYS AND COMPOUNDS

www.elsevier.com/locate/jallcom

Bulk ultra-fine eutectic structure in Ti–Fe–base alloys

J. Das [a,b,*], K.B. Kim [a,c], F. Baier [a], W. Löser [b], A. Gebert [b], J. Eckert [a]

[a] *FG Physikalische Metallkunde, FB 11 Material- und Geowissenschaften, Technische Universität Darmstadt, Petersenstraße 23, D-64287 Darmstadt, Germany*

[b] *Leibniz-Institut für Festkörper- und Werkstoffforschung Dresden, Postfach 270016, D-01171 Dresden, Germany*

[c] *Department of Advanced Materials Engineering, Sejong University, 98 Gunja-dong, Gwangjin-gu, Seoul 143-747, Korea*

Available online 29 September 2006

Abstract

An ultra-fine eutectic structure has been obtained in the $Ti_{70.5}Fe_{29.5}$ binary alloy by slow cooling from the melt through arc melting and cold crucible rod casting. The addition of 3.85 at.% Sn to the binary Ti–Fe alloy induces a change of the morphology of the eutectic and increases the volume fraction of the FeTi (*Pm*3*m*) phase. A significant improvement of the plastic deformability of the ternary alloy has been observed under uniaxial compressive loading resulting in 16% strain to failure compared to 3.4% for binary $Ti_{70.5}Fe_{29.5}$. The morphology of the eutectic colonies, their refinement and supersaturation of the β-Ti phase are crucial factors for improving the ductility of the ultra-fine eutectic alloys.

Keywords: Ultrafine structured materials; Eutectic alloys; Intermetallics; Casting; Mechanical properties

1. Introduction

Usually, metals and alloys having either amorphous structure [1] or nano-/ultrafine grains with narrow size distribution possess high strength but, unfortunately, only rather low ductility at room temperature [2,3]. Attempts have been made to improve the ductility of amorphous alloys [4–6] by introducing heterogeneities with different length-scale and of nanocrystalline materials by tailoring the microstructure through a bimodal grain size distribution [7]. A similar strategy has been followed in order to prepare primary dendrite and nano/ultrafine eutectic microstructures in multicomponent Ti–Cu–Ni–Sn–Nb/Ta [8–10] and Zr–Cu–Ni–Al–Nb alloys [11,12] by casting or in hyper/hypo-eutectic Ti–Fe–Co [13,14] alloys by arc melting. Microcrystalline Ti-alloys have potential use for automotive, aerospace, and biomedical applications [15] due to the low density of the main constituent element Ti (4.5 mg/m^3) and high corrosion resistance [16] but their ultimate strength only slightly exceeds 1000 MPa with plastic strain to failure of 10–15% [17]. The strength of these microcrystalline alloys is quite low compared to the strength (2200 MPa) of brittle Ti–Ni–Cu–Sn bulk glass alloys [18].

However, all the above mentioned nano/ultrafine structured eutectic alloys require micrometer-size β-Ti (Nb/Ta) [8–10] or pro-eutectic FeTi(Co) [13–14] ductile dendritic phases for improvement of the ductility. However, it would be desirable to develop high-strength and ductile eutectic alloys without any micrometer-size second phase dispersions, since such alloys have better castability because of their single melting temperature [19].

In this paper we report on the formation of a nano/ultrafine high-strength ductile eutectic in Ti–Fe and Ti–Fe–Sn alloys in bulk scale through arc melting. The addition of Sn to the binary $Ti_{70.5}Fe_{29.5}$ eutectic alloy changes the morphology of the eutectic during solidification, refines the microstructure and improves the ductility compared to the binary alloy.

2. Experimental

Master alloys were prepared from Ti, Fe and Sn elements of 99.99 wt. % purity by arc melting under an argon atmosphere on a water-cooled Cu hearth. The binary alloy of composition (A) $Ti_{70.5}Fe_{29.5}$ was prepared and co-melted with appropriate portions of Sn to obtain the ternary alloy (B) with composition $Ti_{67.79}Fe_{28.36}Sn_{3.85}$. From these button shape master alloy ingots (40 mm diameter and 10 mm height), rods with 6 mm diameter (Ø) and 85 mm length were solidified in a Cu mold under Ar atmosphere by using a Hukin-type cold-crucible levitation facility. Structural investigations were carried out by X-ray diffraction (XRD) with Cu Kα radiation, a Zeiss DSM 962 scanning electron microscope (SEM), and transmission electron microscopy coupled with energy-dispersive X-ray analysis.

The mechanical properties were evaluated under compression. For this, cylindrical specimens (3 mm diameter) from the as-cast rods and square cross-

* Corresponding author. Present address: FW Dresden, Institut für Festkörperanalytik und Strukturforschung (IFS), Postfach 27 01 16, D-01171 Dresden, Germany. Tel.: +49 351 4659 314; fax: +49 351 4659 452.

E-mail address: j.das@ifw-dresden.de (J. Das).

0925-8388/$ – see front matter © 2006 Elsevier B.V. All rights reserved.
doi:10.1016/j.jallcom.2006.08.163

section (a = 1.6–2.0 mm) specimens from arc melted ingots both with an aspect ratio ~2 were prepared and tested in a Schenck hydraulic testing machine under quasistatic loading at an initial strain rate of $8 \times 10^{-4}\ s^{-1}$ at room temperature.

3. Results and discussion

The XRD patterns of differently prepared Ti–Fe(Sn) alloys are presented in Fig. 1. All the alloys show the presence of bcc β-Ti (A2) and FeTi (B2) reflections. In the case of the as-cast rods and the ingot of the $Ti_{67.79}Fe_{28.36}Sn_{3.85}$ alloy, the relative intensity of the β-Ti reflections is smaller than for the $Ti_{70.5}Fe_{29.5}$ alloy specimens indicating a decrease in the volume fraction of the β-Ti phase due to addition of Sn. Rietvelt refinement [20] yields the lattice parameters of the phases in the different specimens: a_0 = 0.3165 nm (β-Ti) and a_0 = 0.2995 (FeTi) in the as-cast rod, and a_0 = 0.3184 (β-Ti) and a_0 = 0.2994 (FeTi) in the arc melted ingot of the $Ti_{70.5}Fe_{29.5}$ alloy. These lattice parameter values are smaller than the values for pure β-Ti, a_0 = 0.3311 nm, (*Im3m*) and larger than for the equiatomic FeTi phase, a_0 = 0.2975 nm (*Pm3m*) [21]. In the case of the $Ti_{67.79}Fe_{28.36}Sn_{3.85}$ alloy the lattice parameter of the phases are: a_0 = 0.3263 nm (β-Ti) and a_0 = 0.2988 (FeTi) for the as-cast rod, and a_0 = 0.3257 (β-Ti) and a_0 = 0.2989 (FeTi) for the arc-melted ingot. This indicates that there is an increase in the difference between the lattice parameters values (δ) of the A2 and B2 structures from 0.018 nm (binary alloy) to 0.028 nm (ternary alloy) irrespective of the solidification method. The volume fractions of the FeTi phases is estimated to be 24–29 vol.% for $Ti_{70.5}Fe_{29.5}$ and 35–36 vol.% for $Ti_{67.79}Fe_{28.36}Sn_{3.85}$, respectively, indicating an increase by about ~10 vol.% of the FeTi phase due to addition of Sn.

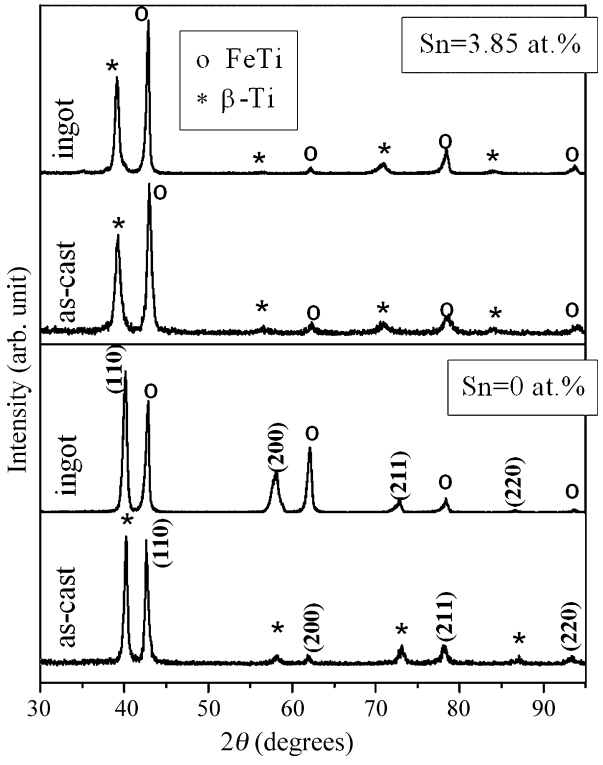

Fig. 1. XRD patterns for $(Ti_{0.705}Fe_{0.295})_{100-x}\ Sn_x$ (x = 0 and 3.85) as-cast rods and arc-melted ingots.

The microstructures of the investigated alloys are quite different concerning their morphologies. Fig. 2 shows cross-sectional SEM back scattered electron images of the differently solidified alloys revealing the presence of the FeTi (white) and β-Ti (Fe/Sn) (dark) phases comprising the eutectic microstructure. For the $Ti_{70.5}Fe_{29.5}$ ingot, directional growth of eutectic colonies was observed from the bottom surface of the specimen (near the Cu hearth) up to a height of ~4 mm. A magnified image of this zone is presented in Fig. 2(a) showing faulted growth of the FeTi phase with a width of 400 nm coexisting with β-Ti(Fe) lamellae. The eutectic spacing (λ) in this zone is about 1 μm. Beyond this region an equiaxed colony structure with 20–50 μm diameter was observed (inset in Fig. 2(a)). Interestingly, the growth of few FeTi particles having a dendritic morphology was also found in this region. This indicates that the growth rate of the FeTi phase (B2) is probably higher than that of the β-Ti(Fe) [A2] phase. In contrast, the $Ti_{67.79}Fe_{28.36}Sn_{3.85}$ ingot exhibits a layer of a 20–100 μm thick chilled microstructure with globular morphology of both β-Ti and FeTi phases. The rest of the cross section shows a homogeneous lamellar eutectic microstructure with oval-shape colonies of 20–50 μm in size. In this case, the colony boundaries are more pronounced than for the binary alloy, as depicted in Fig. 2(b). The eutectic phases exhibit a quite well developed lamellar structure at the center of the colony followed by a radial growth zone and finally a globular-shape appearance of the FeTi phase at the colony boundaries.

In contrast, the as-cast $Ti_{70.5}Fe_{29.5}$ rod shows directional growth of eutectic colonies in a rim of about 50 μm thickness near the rod surface, but homogeneously distributed equiaxed eutectic colonies in the remaining part of the cross section. The brighter phase (FeTi) grows from a common center into radial direction [Fig. 2(c)]. The average eutectic cell size is 20 ± 5 μm without distinct colony boundaries. The eutectic rod spacing (λ) is on the order of 525 nm. EDX analysis of TEM specimens allowed identifying the rod-shape Fe-rich bright phase areas as FeTi (B2) phase, which is embedded in the β-Ti (A2) phase appearing dark in the SEM micrographs. The compositions of the β-Ti and FeTi phases in the binary alloy are $Ti_{77.7}Fe_{22.3}$ and $Ti_{52.7}Fe_{47.3}$, respectively, as determined by EDX analysis. This matches with the solubility of Fe at the eutectic point at 1358 K, which is 22 at.% in β-Ti and 47.5 at.% in the FeTi phase according to the phase diagram [22]. On the other hand, the as-cast $Ti_{67.79}Fe_{28.36}Sn_{3.85}$ rod exhibits a 30–60 μm thick chilled region alike the arc-melted ingot and a homogeneous eutectic microstructure with oval-shape colonies with pronounced colony boundaries and a cell size of 50–10 μm all the way from the surface to the center of the sample [Fig. 1(b)]. The growth of the FeTi phase is rather parallel at the center of the colonies with an interlamellar spacing of 300 nm. At the colony boundaries the growth of the FeTi phase becomes restricted in the longitudinal direction and becomes coarser showing features of impurity segregation. The FeTi lamellae evaluated in this ternary alloy are somewhat thicker than for $Ti_{70.5}Fe_{29.5}$. The morphology of the overall

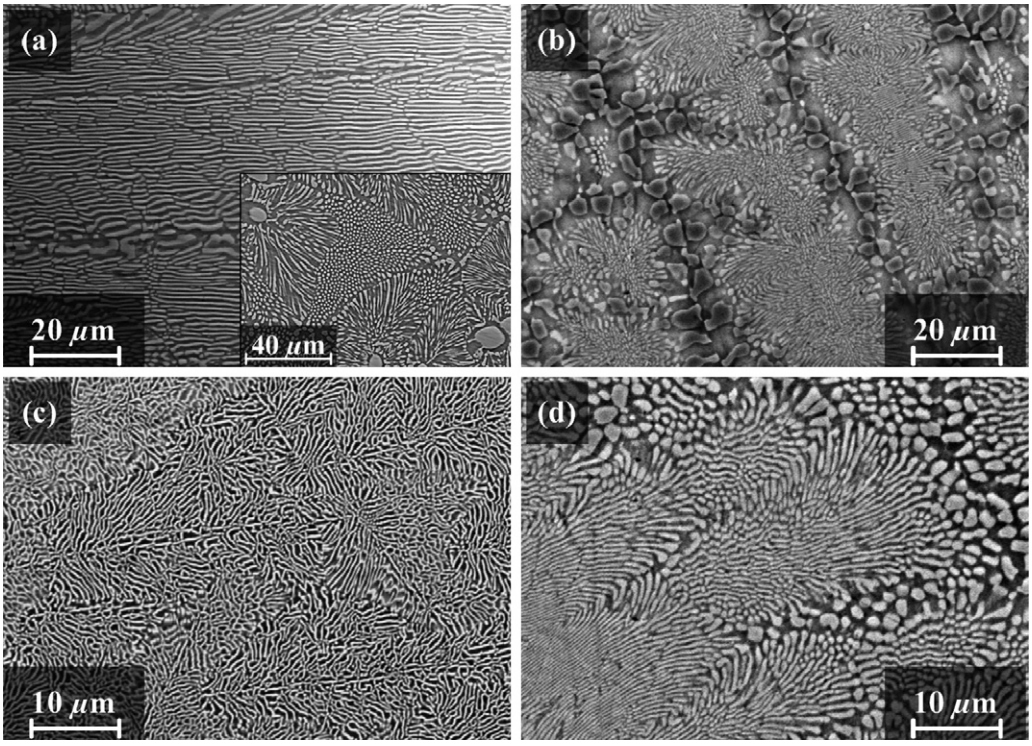

Fig. 2. SEM back scattered electron images of: (a) $Ti_{70.5}Fe_{29.5}$ ingot (near the Cu hearth), inset (near air-cooled region); (b) $Ti_{67.79}Fe_{28.36}Sn_{3.85}$ ingot; (c) $Ti_{70.5}Fe_{29.5}$ as-cast rod; (d) $Ti_{67.79}Fe_{28.36}Sn_{3.85}$ as-cast rod. The micrographs clearly reveal the change in morphology of the eutectic up on Sn addition.

microstructure suggests an increase in the volume fraction of the plate-shape FeTi phase in $Ti_{67.79}Fe_{28.36}Sn_{3.85}$ compared to $Ti_{70.5}Fe_{29.5}$. EDX analysis under TEM conditions revealed that the compositions of β-Ti and FeTi are $Ti_{82.3}Fe_{9.2}Sn_{8.5}$ and $Ti_{52.5}Fe_{46.8}Sn_{0.7}$, respectively, indicating a limited solubility of Sn in the FeTi phase and substitution of Fe by Sn in the β-Ti solid solution.

Fig. 3 presents the engineering stress-strain curves obtained form the uniaxial compression tests under quasistatic loading at an initial strain rate of 8×10^{-4}/s. Since there are microstructural differences between the bottom (near the Cu-hearth) and the top (near the air cooled surface) for the $Ti_{70.5}Fe_{29.5}$ ingot,

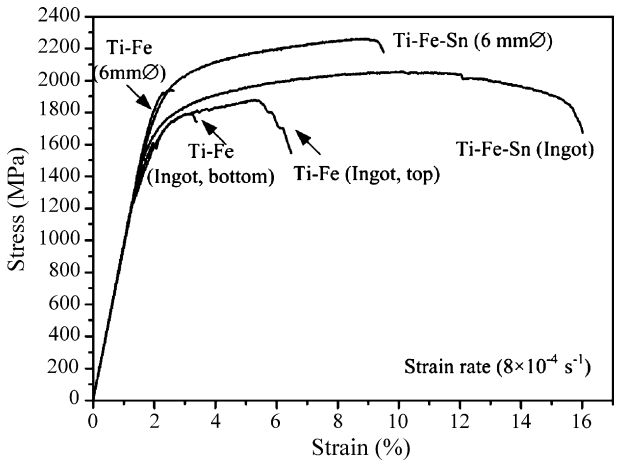

Fig. 3. Room temperature compressive engineering stress–strain curves of the $Ti_{70.5}Fe_{29.5}$ and $Ti_{67.79}Fe_{28.36}Sn_{3.85}$ ingots and as-cast rods.

specimens for the compression tests have been prepared separately from these two different regions. The yield strength of the $Ti_{70.5}Fe_{29.5}$ ingot varies between 1475 MPa (bottom) and 1538 MPa (top). The specimen taken from the bottom part of the ingot failed just after yielding with a plastic strain of only $\varepsilon_p = 1.6\%$ and reaches a fracture stress of about 1790 MPa. In contrast, the specimen taken from the top part of the ingot near to the air cooled surface (Fig. 3, top) shows a higher plastic strain $\varepsilon_p = 4.7\%$ prior to failure at $\sigma_{max} = 1874$ MPa. This may be due to the presence of the micrometer-size FeTi particles [inset, Fig. 2(a)] in the eutectic matrix. For the as-cast $Ti_{70.5}Fe_{29.5}$ sample, the yield strength ($\sigma_y = 1885$ MPa) is higher than the value of $\sigma_y = 1538$ MPa found for arc-melted sample (Table 1) with 0.5% plastic strain. The increase of the yield strength for the as-cast sample can be correlated with the equiaxed eutectic structure with fine inter-lamellar spacing ($\lambda = 525$ nm) in comparison to that of ($\lambda = 1$ μm) the arc-melted ingot. In contrast, we observed no distinct plastic deformability for the $Ti_{70.5}Fe_{29.5}$ binary alloy with homogeneous eutectic microstructure irrespective of the cooling rate or the solidification route applied, as it was observed earlier [23]. Moreover, the as-cast $Ti_{67.79}Fe_{28.36}Sn_{3.85}$ rods with 6 mm diameter exhibits a significantly improved ductility reaching a strain to failure of $\varepsilon_f = 9.6\%$ compared with $\varepsilon_f = 2.6\%$ for the as-cast $Ti_{70.5}Fe_{29.5}$ rods. This ductile sample shows a yield strength of $\sigma_y = 1885$ MPa and work-hardening up 2260 MPa. In addition, the arc-melted ingot shows yielding at 1608 MPa and work-hardening up to 2056 MPa with a notable strain of 16% before failure (Fig. 3). This indicates the superiority of the highly processable (cooling rate of 10 K/s [12]) ternary alloy offering a high ductility for a nano/ultrafine eutectic microstructure, which

Table 1
Room temperature compression test results for $(Ti_{0.705}Fe_{0.295})_{100-x}$ Sn_x ($x = 0$ and 3.85): Young's modulus E, yield stress σ_y, yield strain ε_y, ultimate compression stress σ_{max}, and fracture strain ε_f

Alloy composition	E (GPa)	σ_y (MPa)	ε_y (%)	σ_{max} (MPa)	ε_f (%)
$Ti_{70.5}Fe_{29.5}$ (rod, 6 mm Ø)	95	1885	2.1	1935	2.6
$Ti_{70.5}Fe_{29.5}$ (ingot, top)	95	1475	1.8	1874	6.5
$Ti_{70.5}Fe_{29.5}$ (ingot, bottom)	97	1538	1.8	1791	3.4
$Ti_{67.79}Fe_{28.36}Sn_{3.85}$ (rod, 6 m Ø)	96	1794	2.1	2260	9.6
$Ti_{67.79}Fe_{28.36}Sn_{3.85}$ (ingot)	96	1608	1.9	2056	16.0

does not need any other micrometer-size dendritic phase [8–10] or pro-eutectic FeTi(Co)-phase [13,14] in order to toughen the material.

The remarkable improvement in strength and the range of plastic deformability in the ternary alloy is due to the addition of Sn, which changes the morphology of the eutectic during solidification [24]. Moreover, the Goldschmidt atomic radius of Sn is quite large (0.145 nm) [25], which may establish a long-rage diffusion boundary ahead of the solid/liquid interface, that can destabilize the morphology of the eutectic in the ternary alloy. The addition of Sn limits the solubility of Fe in the β-Ti phase, as determined from EDX analysis and increases the volume fraction of the FeTi phase by about 10 vol.% compared to the binary alloy. The change in the morphology of the eutectic and the high coherency strain due to the lattice mismatch ($\delta = 0.028$ nm) between the A2 and B2 structures, may enhance the ductility and provide better slip transfer to accommodate the applied strain rather than initiating cleavage at the A2/B2 interface [24].

4. Conclusions

Nano/ultrafine microstructures have been produced in Ti–Fe/(Sn) eutectic alloys. The addition of Sn changes the morphology of the eutectic and the lattice parameter of the β-Ti phase without altering the lattice parameter of the FeTi phase. High strength–ductile bulk specimens with ultrafine eutectic microstructure can be obtained after adding the rather cheap element Sn to binary $Ti_{70.5}Fe_{29.5}$ alloy. The ingot of the $Ti_{67.79}Fe_{28.36}Sn_{3.85}$ alloy solidified at a low cooling rate (10 K/s) shows the high processability of this ductile alloy in bulk scale without any micrometer-size second phase dispersions.

Acknowledgements

The authors thank S. Kuszinski, G. Miehe, H. Schulze, and R. Theissmann for technical assistance and simulating discussions and U. Kunz for TEM sample preparation. The authors are grateful for the financial support provided by the European Union within the framework of the Research Training Network on "ductile bulk metallic glass composites" (MRTN-CT-2003-504692).

References

[1] H.A. Bruck, T. Christman, A.J. Rosakis, W.L. Johnson, Scripta Metall. Mater. 30 (1994) 429.
[2] C.C. Koch, Nanostructured Materials: Processing Properties and Applications, Noyes Publishing/William Andrew Publishing, Norwich, NY, 2002, p. 3.
[3] C.C. Koch, J. Metast. Nanocryst. Mater. 18 (2003) 9.
[4] J. Das, M.B. Tang, K.B. Kim, R. Theissmann, F. Baier, W.H. Wang, J. Eckert, Phys. Rev. Lett. 94 (2005) 205501.
[5] C.C. Hays, C.P. Kim, W.L. Johnson, Phys. Rev. Lett. 84 (2000) 2901.
[6] U. Kühn, J. Eckert, N. Mattern, L. Schultz, Appl. Phys. Lett. 80 (2002) 2478.
[7] Y. Wang, M. Chen, F. Zhou, E. Ma, Nature 419 (2002) 912.
[8] G. He, J. Eckert, W. Löser, L. Schultz, Nat. Mater. 2 (2003) 33.
[9] G. He, W. Löser, J. Eckert, Acta Mater. 51 (2003) 5223.
[10] G. He, J. Eckert, W. Löser, M. Hagiwara, Acta Mater. 52 (2004) 3035.
[11] J. Das, W. Löser, U. Kühn, J. Eckert, S.K. Roy, L. Schultz, Appl. Phys. Lett. 82 (2003) 4690.
[12] J. Das, A. Güth, H.-J. Klauß, C. Mickel, W. Löser, J. Eckert, S.K. Roy, L. Schultz, Scripta Mater. 49 (2003) 1189.
[13] D.V. Louzguine, H. Kato, A. Inoue, Philos. Mag. Lett. 84 (2004) 359.
[14] D.V. Louzguine, L.V. Louzguina, H. Kato, A. Inoue, Acta. Mater. 53 (2005) 2009.
[15] G. Lütjering, J. Albrecht, Ti-2003 Science and Technology, Vol. 1, Wiley-Vch Verlag GmbH & Co, 2003, p.1.
[16] S. Parlapanska, D. Parlapanski, Corros. Sci. 39 (1977) 1321.
[17] E.A. Brandes, G.B. Brook (Eds.), Smithells Metals Reference Book, 7th ed., Butterworth–Heinemann Ltd., Hartnolls Ltd., Bodmin, U.K, 1992, p. p22.
[18] T. Zhang, A. Inoue, Mater. Trans. JIM 39 (1998) 1001.
[19] W. Kurz, D.J. Fisher, Fundamentals of Solidification, 4th ed., Trans Tech Publications, 1998.
[20] R.A. Young, Introduction to the Rietveld Method, Oxford University Press, Oxford, 1993.
[21] PCPDFWIN Version 2.2, JCPDS-International Centre for Diffraction Data, 2001.
[22] T.B. Massalski, H. Okamoto, P.R. Subramanian, L. Kasprzak, Binary Alloy Phase Diagrams, 2nd ed., ASM International, 1992, p. 1783.
[23] D.V. Louzguine, H. Kato, L.V. Louzguina, A. Inoue, J. Mater. Res. 19 (2004) 3600.
[24] J. Das, K.B. Kim, F. Baier, W. Löser, J. Eckert, Appl. Phys. Lett., submitted for publication.
[25] E. Clementi, D.L. Raimondi, W.P. Reinhardt, J. Chem. Phys. 38 (1963) 2686.